Effect of neutron skin thickness on projectile fragmentation

Z. T. Dai (代智涛),[1,2] D. Q. Fang (方德清),[1,*] Y. G. Ma (马余刚),[1,3,†] X. G. Cao (曹喜光),[1]
G. Q. Zhang (张国强),[1] and W. Q. Shen (沈文庆)[1]

[1]*Shanghai Institute of Applied Physics, Chinese Academy of Sciences, Shanghai 201800, China*
[2]*University of Chinese Academy of Sciences, Beijing 100049, China*
[3]*Shanghai Tech University, Shanghai 200031, China*

(Received 13 November 2014; revised manuscript received 2 February 2015; published 30 March 2015)

The fragment production in collisions of ^{48,50}Ca+^{12}C at 50 MeV/nucleon are simulated via the isospin-dependent quantum molecular dynamics (IQMD) model followed by the GEMINI code. By changing the diffuseness parameter of neutron density distribution to obtain different neutron skin sizes, the effects of neutron skin thickness (δ_{np}) on projectile-like fragments (PLFs) are investigated. The sensitivity of isoscaling behavior to neutron skin size is studied, from which it is found that the isoscaling parameter α has a linear dependence on δ_{np}. A linear dependence between δ_{np} and the mean N/Z [N (Z) is neutron (proton) number] of the PLF is obtained as well. The results show that thicker neutron skin will lead to smaller isoscaling parameter α and N/Z. Therefore, it may be probable to extract information of neutron skin thickness from isoscaling parameter α and N/Z.

DOI: 10.1103/PhysRevC.91.034618 PACS number(s): 21.10.Gv, 24.10.−i, 25.70.Mn

I. INTRODUCTION

The neutron skin of a nucleus has been one of the hottest issues in nuclear physics. It is defined as the difference between the neutron and proton rms radii: $\delta_{np} = \langle r_n^2\rangle^{1/2} - \langle r_p^2\rangle^{1/2}$. The mechanism for the formation of neutron skin can be expressed as follows. The proton-neutron interaction is stronger than the proton-proton or neutron-neutron interaction. Therefore, if the neutron number increases for neutron rich nuclei, the mean potential for protons becomes deeper, while the potential for neutrons becomes shallower. Consequently, protons are more deeply bound, but neutrons are more loosely bound, which will form the neutron skin [1]. The neutron skin thickness in neutron rich nuclei is crucial for studying the equation of state (EOS) of asymmetric nuclear matter due to its strong correlations with the symmetry energy and the slope and curvature of symmetry energy at the saturation density [2–10]. Thus neutron skin thickness and its effect in nuclear reactions becomes an important research subject in nuclear physics.

Using the isospin-dependent quantum molecular dynamics (IQMD) model, Sun *et al.* investigated the neutron to proton ratio [$R(n/p)$] of emitted fragments from projectiles with different neutron skin thicknesses and shown that there is a strong linear correlation between $R(n/p)$ and δ_{np}, especially for peripheral collisions [11]. Meanwhile, we have investigated the correlation between the ratio of triton to ^{3}He [$R(\mathrm{t}/^3\mathrm{He})$] and δ_{np}, which exhibits the similar linear relation [12]. Projectile fragmentation is a well-established technique for rare isotope productions by many radioactive ion beam facilities in the world. The projectile fragmentation is used not only to study the reaction mechanism of nuclear collisions but also to extract some information on fundamental physics [13–15]. The production of heavy fragments will be affected by the neutron and/or proton density distributions of the projectile nuclei. Thus studies on the effect of neutron skin thickness over the projectile-like fragment (PLF) will be very interesting.

In this paper, the relationship between δ_{np} and average N/Z, the isotope distribution, and the yield ratios of PLF will be studied within the framework of the IQMD model. The paper is organized as follows. In Sec. II, we briefly describe the method, i.e., IQMD model plus GEMINI code. In Sec. III, we present both the results and discussions. Finally, a summary is given in Sec. IV.

II. FRAMEWORK DESCRIPTION

A. Dynamical model: IQMD

The quantum molecular dynamics (QMD) approach is a many-body theory to describe heavy ion collisions from intermediate to relativistic energies. A general review about the model can be found in Refs. [16,17]. The IQMD model is based on the QMD model with the explicit inclusion of isospin degrees of freedom. It is well known that the dynamics at intermediate energies is mainly governed by three parts: the mean field, two-body nucleon-nucleon collisions, and the Pauli blocking. Therefore, it is necessary to include isospin degrees of freedom to the three parts for isospin-dependent dynamics. In initialization of the projectile and target nuclei, neutrons and protons should be sampled separately in phase space, especially for nuclei far away from the β-stability line, of which the neutron and proton density distributions are much different. The QMD model has been widely and successfully used in heavy ion collisions [11,18–29]. Details about the description of the IQMD model can be found in Refs. [11,12].

In the present work, the following potential is used:

$$U(\rho,\tau_z) = \alpha\left(\frac{\rho}{\rho_0}\right) + \beta\left(\frac{\rho}{\rho_0}\right)^{\gamma} + \frac{1}{2}(1-\tau_z)V_c + C_{\mathrm{sym}}\frac{\rho_n-\rho_p}{\rho_0}\tau_z + U^{\mathrm{Yuk}}, \quad (1)$$

where $\rho_0 = 0.16$ fm^{-3} is the normal nuclear matter density. ρ, ρ_n, and ρ_p are the total, neutron, and proton densities,

*dqfang@sinap.ac.cn
†ygma@sinap.ac.cn

respectively. τ_z is the zth component of the isospin degree of freedom, which equals 1 or -1 for neutrons or protons, respectively. The coefficients α, β, and γ are parameters of the nuclear EOS. $C_{\rm sym}$ is the symmetry energy strength due to the difference between neutron and proton asymmetry in nuclei. In this work, $\alpha = -356$ MeV, $\beta = 303$ MeV, and $\gamma = 7/6$ are taken, which corresponds to the so-called soft EOS with an incompressibility of $K = 200$ MeV and $C_{\rm sym} = 32$ MeV. V_c is the Coulomb potential and $U^{\rm Yuk}$ is the Yukawa potential. Many theoretical studies show a strong correlation between symmetry energy and neutron skin size, while there is still large uncertainty of neutron skin size and symmetry energy [30,31]. As discussed in Ref. [32], both the symmetry and neutron skin have effects on particle production. Therefore, it is interesting to study separately the effects of neutron skin and symmetry energy. The correlations between symmetry energy and particle or fragment production have also been investigated in many theoretical studies [32–34]. The flexibility of adjusting independently the size of the neutron skin of colliding nuclei is useful for our analyses in this work. Moreover, in this work, different neutron skin thicknesses mainly influence the neutron density distribution in the surface region of nuclei, so our study is focused on the peripheral collisions. In the peripheral collisions, the effect of neutron skin is larger than the effect due to the symmetry energy [32].

In the initialization of IQMD, the density distributions of neutrons and protons are assumed to follow the Fermi-type form according to the droplet model [35,36],

$$\rho_i(r) = \frac{\rho_i^0}{1 + \exp\left(\frac{r - C_i}{f_i t_i / 4.4}\right)}, \quad i = n, p, \tag{2}$$

where ρ_i^0 is the normalization constant which ensures that the integration of the density distribution equals the number of neutrons ($i = n$) or protons ($i = p$); t_i is the diffuseness parameter; and C_i is the half density radius of neutron or proton determined by the droplet model [36], i.e.,

$$C_i = R_i[1 - (b_i/R_i)^2], \quad i = n, p, \tag{3}$$

here $b_i = 0.413 f_i t_i$, R_i is the equivalent sharp surface radius of neutron or proton. R_i and t_i are given by the droplet model. The factor f_i is used to adjust the diffuseness of density distribution. In this work, $f_p = 1.0$ is used in Eq. (2) for the proton density distribution, while f_n in Eq. (2) is varied from 1.0 to 1.6 for the neutron rich projectile. Different values of δ_{np} can be deduced from Eq. (2) by changing f_n. Using the density distributions given by the droplet model, initial coordinates of nucleons in the nucleus are sampled in terms of the Monte Carlo method. After initialization, the samples with satisfactory stability and the expected neutron skin size will be selected as candidates for collisions, as described in Refs. [11,12]. Figure 1 shows the neutron and proton density profiles of ^{50}Ca calculated from IQMD initialization. In the simulation, f_n is 1.0, 1.2, 1.4, and 1.6, respectively. It can be seen that with the increase of f_n, the neutron density distribution becomes more extended, while that of the proton is almost the same in the four cases. The related neutron skin thicknesses are 0.08, 0.21, 0.37, and 0.54 fm, respectively. The initial neutron skin can last as long as the reaction time, although a small-amplitude oscillation is visible. This level of stability of the initial samples is good enough for the purpose of this study. As a consequence, we can study the neutron skin effect on the production of fragments with these samples. In this work, the fragments are constructed by a coalescence model, in which nucleons with relative momentum smaller than $P_0 = 300$ MeV/c and relative distance smaller than $R_0 = 3.5$ fm will be identified as a cluster.

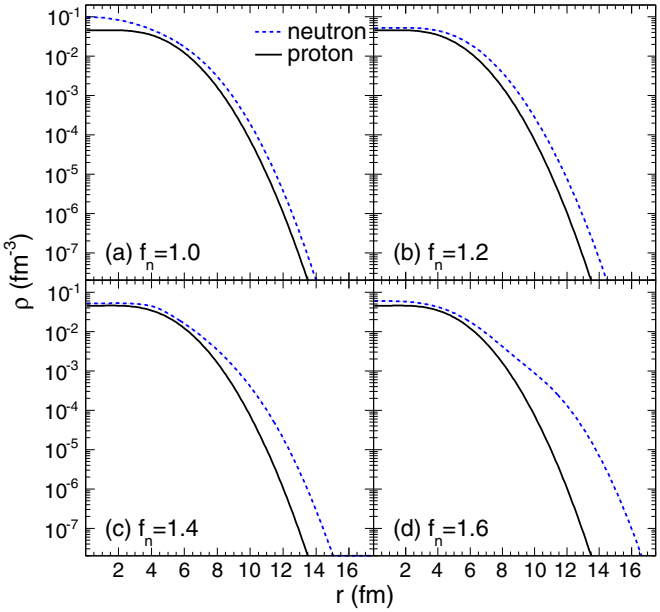

FIG. 1. (Color online) Neutron and proton density profiles calculated from IQMD initialization for ^{50}Ca at $t = 0$ with $f_p = 1.0$ but different f_n. (a) $f_n = 1.0$ ($\delta_{np} = 0.08$ fm); (b) $f_n = 1.2$ ($\delta_{np} = 0.21$ fm); (c) $f_n = 1.4$ ($\delta_{np} = 0.37$ fm); (d) $f_n = 1.6$ ($\delta_{np} = 0.54$ fm).

B. Decay model: GEMINI

The prefragments produced in IQMD are excited, which is not the case with the final products measured experimentally; therefore it is necessary to take into account the evaporation effect to obtain realistic results. The GEMINI code is used to calculate de-excitation of these fragments [37]. GEMINI is a Monte Carlo code which allows not just light-particle evaporation and symmetric fission, but all possible binary-decay modes. It de-excites a source nucleus by a series of sequential binary decays until the excitation energy of the excited fragment is unable to undergo further decay. By using GEMINI, the fragment productions are widely and successfully investigated with the QMD model [38–40], as well as the anti-symmetrized molecular dynamics (AMD) model [41,42]. In IQMD, we can construct the angular momentum and excitation energy for each fragment, which are used as input to GEMINI. The angular momentum of each nucleon in the fragment is calculated according to classical mechanics

$$\vec{L}_i = \vec{R}_i \times \vec{P}_i, \tag{4}$$

where $\vec{R}_i$ and $\vec{P}_i$ are coordinate and momentum vectors of the ith nucleon of the fragment in the center-of-mass frame of the fragment. The total angular momentum of the fragment is the summation of Eq. (4) over all nucleons in it. The excitation

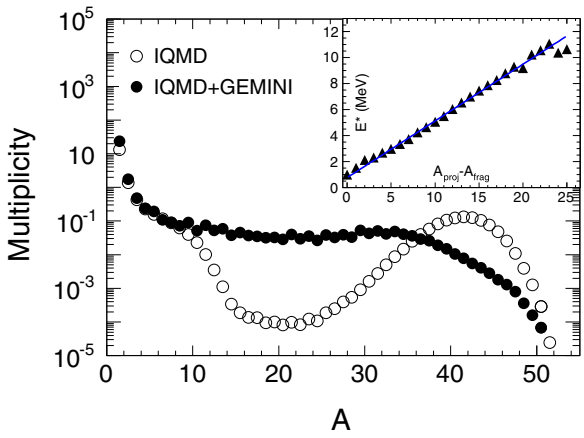

FIG. 2. (Color online) Fragment mass multiplicity distribution in 50 MeV/nucleon ^{50}Ca+^{12}C with $f_n = 1.0$ and $0.6 < b/b_{\max} < 1.0$. Open circles represent IQMD calculation at $t = 200$ fm/c and solid points are results after the evaporation by GEMINI. The excitation energy per nucleon of the prefragment as a function of $A_{\rm proj} - A_{\rm frag}$ calculated by IQMD simulations is shown in the inset.

energy of the primary fragment is calculated by

$$E^* = E^{\rm excited}_{\rm bind} - E^{\rm ground}_{\rm bind}, \quad (5)$$

where $E^{\rm excited}_{\rm bind}$ is the binding energy of the excited fragment calculated from IQMD, and $E^{\rm ground}_{\rm bind}$ is the binding energy of the ground state taken from the nuclear mass table [46]. The inset of Fig. 2 displays E^* as a function of $A_{\rm proj} - A_{\rm frag}$, where A is the mass number and the indices proj and frag refer to the projectile and fragment, respectively. Although the constructed excitation energy is model dependent, the excitation energy obtained from our IQMD calculation is comparable with that constructed from experimental data and model simulations [43–45].

With the calculated excitation energy and angular momentum, the fragments at $t = 200$ fm/c will be de-excited by using GEMINI. Since the main purpose of the present work is to study the effect of neutron skin thickness of the projectile on the production of heavy fragments, the calculations are focused on peripheral collisions. The reduced impact parameter is used to describe the centrality of collisions which is defined as $b/b_{\max}$, with $b_{\max}$ being the maximum impact parameter. For peripheral reactions, the nucleon-nucleon interaction on the nuclear surface plays an important role, where nucleons are loosely bound and the density distributions are quite different for neutron and proton. Figure 2 represents the comparison of mass versus multiplicity of fragments with and without GEMINI decay under the condition of $0.6 < b/b_{\max} < 1.0$. In the peripheral collision of IQMD, the main reaction mechanism of fragment production is abrasion and evaporation of nucleons or light clusters, which leads to the excess of heavy products and deficiency of intermediate mass fragments (IMFs). In contrast, applying the afterburner significantly improves fragment production since more complex fragments are emitted in the de-excitation calculation.

III. RESULTS AND DISCUSSIONS

Before investigating the neutron skin effect in fragment production, the isotopic distributions calculated by IQMD plus GEMINI are compared with experimental data to evaluate the validity of the present method. In Fig. 3 the measured cross sections from Ref. [47] and the calculated results of IQMD plus GEMINI for fragments with $12 \leqslant Z \leqslant 20$ from ^{48}Ca+^{9}Be at 140 MeV/nucleon are plotted. The calculated yields are scaled to the experimental data for each isotope separately. From this comparison, we can see that our calculations can reproduce the shape of the isotopic distribution data quite well, which suggests that the IQMD plus GEMINI model is reasonable for calculating the heavy fragments. This is also demonstrated in Refs. [38,40]. Meanwhile, Mock *et al.* have well reproduced this experimental data with heavy ion phase space exploration (HIPSE), Abrasion-Ablation (AA) and AMD [44,45].

As discussed in Ref. [48], the neutron skin plays a significant role in the production of fragments, especially for the production of neutron rich nuclei. Hence, to reveal the correlation between neutron skin and fragment production is interesting. Using the IQMD model, collisions of ^{48,50}Ca projectile on ^{12}C target at 50 MeV/nucleon are simulated. In our simulations, the diffuseness parameter $f_n = 1.0$ is used for ^{48}Ca, while f_n varies from 1.0 to 1.6 for ^{50}Ca. In the upper row of Fig. 4, the production yield per event for five isotopes with the charge number varying from 15 to 19 are plotted. The reason why we choose the fragments with the charge number varying from 15 to 19 is explained as follows. The main purpose of this work is to study the neutron skin effects on fragments. In our IQMD, the probability of fusion is small, so the fragments with charge numbers larger than the projectile are neglected. The lighter fragments, which reach chemical balance at the end of the reaction, will keep little information of the source nuclei, so the effect of neutron skin thickness on these fragments is very small. While the heavy residue can keep as much information of the projectile as possible. Therefore, fragments with the charge number varying from 15 to 19 are chosen as a probe of neutron skin.

First, we compare the fragment isotopic distributions from reactions induced by projectiles with different neutron excess. By comparing the two systems ^{48}Ca+^{12}C and ^{50}Ca+^{12}C with $f_n = 1.0$, it is demonstrated that there are more neutron rich fragments produced with increasing neutron excess of the projectile. This result is similar to that in Ref. [13]. Second, we compare the reactions ^{50}Ca+^{12}C with different f_n, which relates to different δ_{np}. With the increase of neutron skin thickness, yields of the isotope distributions will decrease in the neutron rich side but have almost no change in the neutron deficient side, which is consistent with the results by the statistical AA model [49].

Meanwhile, it has been shown that the yield ratios of isotopic fragments from two similar reactions that differ only in the isospin asymmetry follow scaling laws [50–56]. The isotope yield ratios $R_{21}(N,Z) = Y_2(N,Z)/Y_1(N,Z)$ measured in two different nuclear reactions (indices 1 and 2) are found to exhibit an exponential relationship as a function of the neutron number N and proton number Z [50], which can be expressed

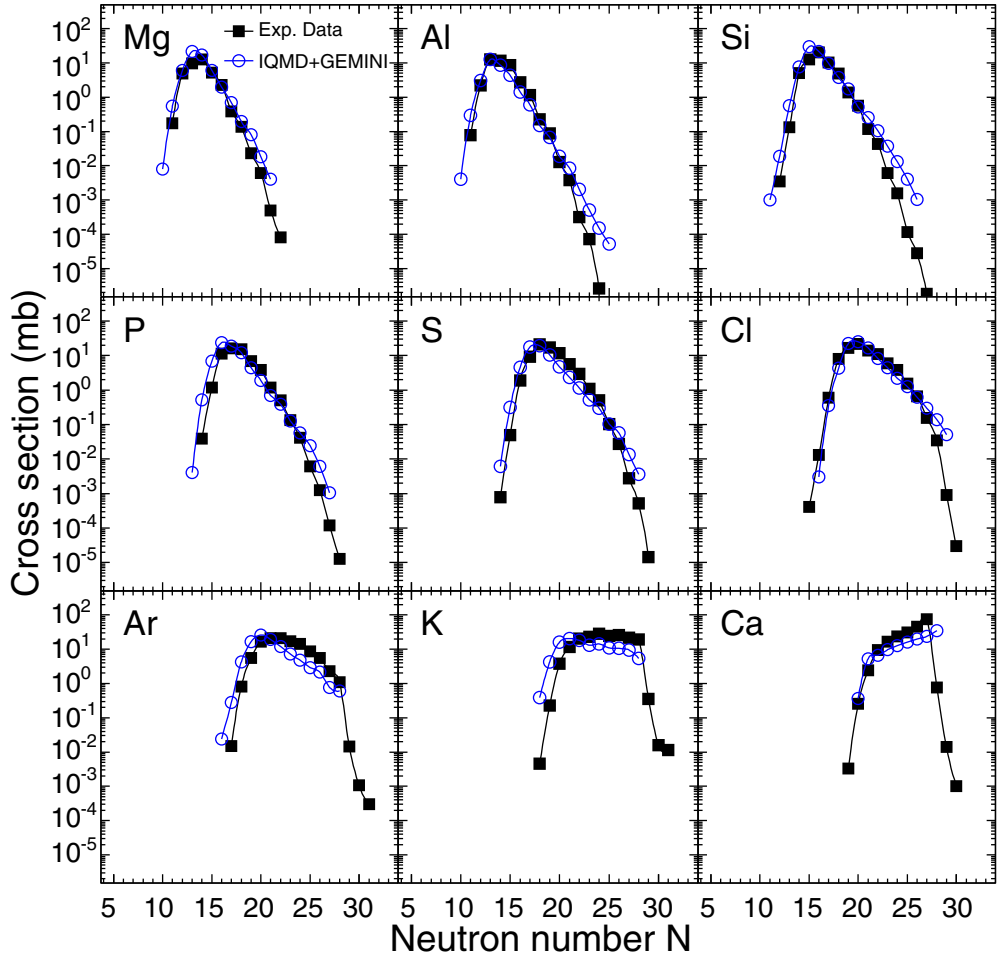

FIG. 3. (Color online) Isotopic distributions as a function of neutron number N for elements with $12 \leqslant Z \leqslant 20$ in 140 MeV/nucleon ^{48}Ca+^{9}Be. Solid squares are the experimental data from Ref. [47], and open circles are the calculated results with IQMD plus GEMINI.

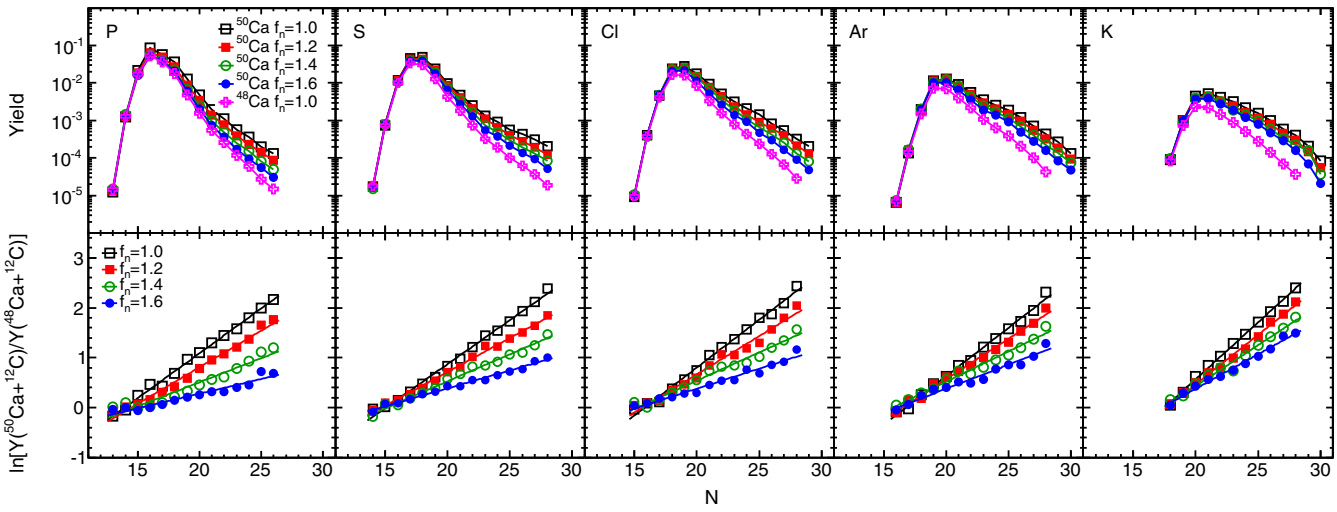

FIG. 4. (Color online) Isotopic yield per event as a function of the neutron number N with the charge number of fragment varying from 15 to 19 in ^{50}Ca+^{12}C and ^{48}Ca+^{12}C at 50 MeV/nucleon (upper row). The related isotopic yield ratios of the two reactions as functions of N are displayed in the lower row. In the calculations, f_n is varied from 1.0 to 1.6 for ^{50}Ca+^{12}C, while it is 1.0 for ^{48}Ca+^{12}C.

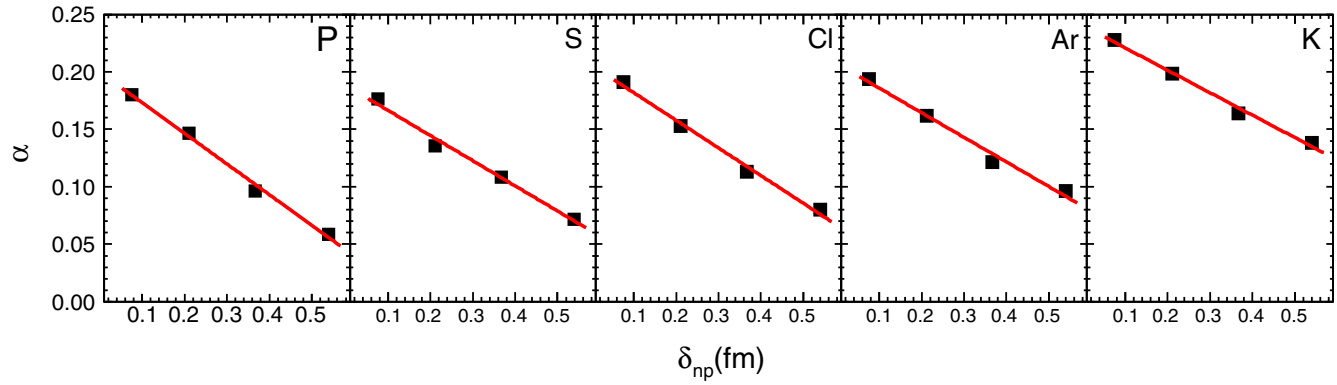

FIG. 5. (Color online) Isoscaling parameter α as a function of δ_{np} for fragments with the charge number varying from 15 to 19 in 50 MeV/nucleon ^{50}Ca+^{12}C.

by following formula:

$$R_{21}(N,Z) = \frac{Y_2(N,Z)}{Y_1(N,Z)} = C\exp(\alpha N + \beta Z), \qquad (6)$$

where α and β are two scaling parameters and C is an overall normalization constant.

The isoscaling phenomenon is systematically investigated for fragments not heavier than $Z = 8$. However, it would be interesting to investigate the behavior of heavier fragments up to the region of PLFs, because the heavy residues, which are mainly produced by abrasion and evaporating mechanisms, may preserve some memory of the source configuration, for example, the neutron and proton density distribution. The isotopic scaling of heavy projectile residues is observed in both experiment and theoretical simulation [54–58]. Consequently, from the research of isoscaling of heavy residues of the projectile, some information about the neutron skin of a neutron rich projectile could be extracted, since the neutron skin does effect the production of fragments [48]. This is our new starting point. In order to investigate the neutron skin size effect on isoscaling, the isotopic yield ratios between two reactions ^{50}Ca+^{12}C and ^{48}Ca+^{12}C are plotted as a function of the fragment neutron number, as shown in the lower row of Fig. 4. In the calculation, $f_n = 1.0$ is used for ^{48}Ca, while $f_n = 1.0, 1.2, 1.4$ and 1.6 are used for ^{50}Ca. From the figure, we can see that a larger neutron skin size will suppress the production of the neutron rich fragment. Although the neutron number and proton number of projectiles and targets are not changed in the reactions ^{50}Ca+^{12}C and ^{48}Ca+^{12}C, the neutron density of ^{50}Ca is different with different f_n. Equation (6) can be simplified for isotopic yield ratios with the same charge number,

$$R_{21}(N) = C'\exp(\alpha N). \qquad (7)$$

In the grand-canonical approximation, the scaling parameter α is equal to the difference of the chemical potentials for neutrons in the two systems, $\alpha = \mu_n/T$ [50,51]. The parameter α is extracted by fitting $\ln[R_{21}(N,Z)]$ as a function of N. α dependence on δ_{np} for isotopes with proton numbers varying from $Z = 15$ to $Z = 19$ is displayed in Fig. 5. One can see that α decreases linearly with increasing neutron skin thickness in the projectile. It is indicated that the scaling parameter does not keep constant for the heavy residues with proton numbers close to the projectile, which is different from that for light fragments. This different isoscaling behavior between heavy and light fragments may result from different formation dynamics. The light fragments are mainly produced from multi-fragmentation, in which the system has reached chemical balance, which leads to the similar isoscaling behavior of light fragments. While the heavy residues close to the projectile originate from nucleon abrasion or evaporation. In this case, most of the nucleons in the projectile may only act as spectators, and accordingly, the system is not balanced. Nevertheless, the heavy residues will keep a memory of the projectile to some degree. From this result some information of neutron skin could be extracted by measuring the isoscaling behavior of the heavy residues.

Finally, the neutron skin effect on N/Z of heavy PLF is also investigated. The average N/Z for PLFs with charge numbers from $Z = 15$ to $Z = 19$ as a function of δ_{np} are plotted in Fig. 6. It displays that N/Z decreases with the increasing of δ_{np}, and there is a good linear correlation between N/Z and δ_{np}. This relationship could be regard as another probe for neutron skin thickness. We also can see that for a certain

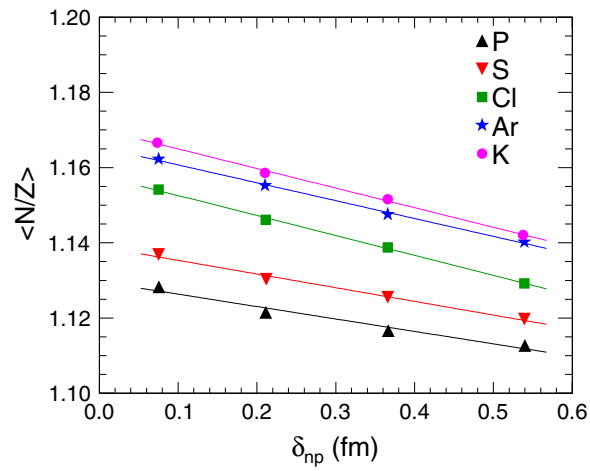

FIG. 6. (Color online) Average N/Z of fragments as a function of δ_{np} in 50 MeV/nucleon ^{50}Ca+^{12}C.

δ_{np}, the N/Z will increase with the increasing charge number, which is similar to the results in Ref. [58].

The neutron skin effect on fragment production, isoscaling, and N/Z of residues could be explained as follows. For different neutron skin thicknesses, the main differences in neutron density distributions are in the surface region. With increasing of δ_{np}, more neutrons are pushed to the surface of the nuclei. Consequently, more neutrons will be abraded in peripheral collisions, which makes the residue less neutron rich. Large δ_{np} makes the neutron become more loosely bound, and more neutrons will be evaporated.

IV. SUMMARY

Using the isospin-dependent quantum molecular dynamics (IQMD) model followed by GEMINI, the neutron skin effect on the production of projectile-like fragments are investigated in peripheral collisions of 50 MeV/nucleon ^{50}Ca+^{12}C and ^{48}Ca+^{12}C. By changing the neutron diffuseness parameter of ^{50}Ca to obtain different neutron skin thicknesses (δ_{np}), the dependence of isotopic distributions, neutron to proton ratios (N/Z), and isoscaling behaviors of PLFs on δ_{np} is studied. It is demonstrated that larger δ_{np} suppresses the production of neutron rich PLFs. This is because projectiles with larger δ_{np} prefer to produce more free neutrons and neutron rich light clusters. The isoscaling behavior in ^{50}Ca+^{12}C and ^{48}Ca+^{12}C are also investigated. The extracted isoscaling parameter α decreases linearly with the increase of δ_{np}. The dependence of the N/Z of the PLF on δ_{np} displays a similar trend. With the increase of δ_{np}, more neutrons will distribute in the nuclear surface. Consequently, they will be abraded in peripheral collisions more easily. In conclusion, the isotopic distributions, isoscaling parameter α, and neutron to proton ratios N/Z of PLFs have dependence on δ_{np}. This dependence could probably be used to extract some information on neutron skin from experiments.

ACKNOWLEDGMENTS

This work was supported in part by the Major State Basic Research Development Program in China under Contract No. 2013CB834405, the National Natural Science Foundation of China under Contracts No. 11175231, No. 11035009, No. 11475244, No. 11421505, and No. 11205079, and the Knowledge Innovation Project of CAS under Grant No. KJCX2-EW-N01.

[1] N. Fukunishi, T. Otsuka, and I. Tanihata, Phys. Rev. C **48**, 1648 (1993).
[2] B. A. Brown, Phys. Rev. Lett. **85**, 5296 (2000).
[3] C. J. Horowitz and J. Piekarewicz, Phys. Rev. Lett. **86**, 5647 (2001).
[4] C. J. Horowitz and J. Piekarewicz, Phys. Rev. C **66**, 055803 (2002).
[5] S. Typel and B. A. Brown, Phys. Rev. C **64**, 027302 (2001).
[6] R. J. Furnstahl, Nucl. Phys. A **706**, 85 (2002).
[7] S. Karataglidis, K. Amos, B. A. Brown, and P. K. Deb, Phys. Rev. C **65**, 044306 (2002).
[8] M. Centelles, X. Roca-Maza, X. Viñas, and M. Warda, Rev. Lett. **102**, 122502 (2009).
[9] A. Carbone, G. Colò, A. Bracco, L.-G. Cao, P. F. Bortignon, F. Camera, and O. Wieland, Phys. Rev. C **81**, 041301(R) (2010).
[10] F. J. Fattoyev and J. Piekarewicz, Phys. Rev. Lett. **111**, 162501 (2013).
[11] X. Y. Sun, D. Q. Fang, Y. G. Ma, X. Z. Cai, J. G. Chen, W. Guo, W. D. Tian, and H. W. Wang, Phys. Lett. B **682**, 396 (2010).
[12] Z. T. Dai, D. Q. Fang, Y. G. Ma, X. G. Cao, and G. Q. Zhang, Phys. Rev. C **89**, 014613 (2014).
[13] D. Q. Fang, W. Q. Shen *et al.*, Phys. Rev. C **61**, 044610 (2000).
[14] Y. G. Ma, Q. M. Su, W. Q. Shen, D. D. Han, J. S. Wang, X. Z. Cai, D. Q. Fang, and H. Y. Zhang, Phys. Rev. C **60**, 024607 (1999).
[15] S. Lukyanov, M. Mocko *et al.*, Phys. Rev. C **80**, 014609 (2009).
[16] J. Aichelin, A. Rosenhauer, G. Peilert, H. Stöcker, and W. Greiner, Phys. Rev. Lett. **58**, 1926 (1987).
[17] C. Hartnack, R. K. Puri, J. Aichelin, J. Konopka, S. A. Bass, H. Stöcker, and W. Greiner, Eur. Phys. J. A **1**, 151 (1998).
[18] X. G. Cao, X. Z. Cai, Y. G. Ma, D. Q. Fang, G. Q. Zhang, W. Guo, J. G. Chen, and J. S. Wang, Phys. Rev. C **86**, 044620 (2012).
[19] J. Y. Liu, W. J. Guo, Z. Z. Ren, X. Z. Xing, W. Zuo, and X. G. Lee, Phys. Lett. B **617**, 24 (2005).
[20] C. Tao, Y. G. Ma, G. Q. Zhang, X. G. Cao, D. Q. Fang, and H. W. Wang, Phys. Rev. C **87**, 014621 (2013); Nucl. Sci. Techniques **24**, 030502 (2013); J. Wang, Y. G. Ma, G. Q. Zhang, D. Q. Fang, L. X. Han, and W. Q. Shen, *ibid.* **24**, 030501 (2013).
[21] Y. G. Ma and W. Q. Shen, Phys. Rev. C **51**, 710 (1995).
[22] F. S. Zhang, L. W. Chen, Z. Y. Ming, and Z. Y. Zhu, Phys. Rev. C **60**, 064604 (1999).
[23] Y. G. Ma and W. Q. Shen, Phys. Rev. C **51**, 3256 (1995).
[24] Y. G. Ma, Y. B. Wei *et al.*, Phys. Rev. C **73**, 014604 (2006).
[25] C. L. Zhou, Y. G. Ma, D. Q. Fang, and G. Q. Zhang, Phys. Rev. C **88**, 024604 (2013).
[26] Y. X. Zhang, L. Z. Xia *et al.*, Nucl. Sci. Techniques **24**, 050503 (2013).
[27] Z. Q. Feng, Nucl. Sci. Techniques **24**, 050504 (2013).
[28] S. Kummar and Y. G. Ma, Nucl. Sci. Techniques **24**, 050509 (2013).
[29] C. C. Guo, J. Su, and F. S. Zhang, Nucl. Sci. Techniques **24**, 050513 (2013).
[30] B. K. Agrawal, J. N. De, and S. K. Samaddar, Phys. Rev. Lett. **109**, 262501 (2012).
[31] M. B. Tsang, Y. X. Zhang, P. Danielewicz, M. Famiano, Zhuxia Li, W. G. Lynch, and A. W. Steiner, Phys. Rev. Lett. **102**, 122701 (2009).
[32] G. F. Wei, B. A. Li, Jun Xu, and Lie-Wen Chen, Phys. Rev. C **90**, 014610 (2014).
[33] Sanjeev Kumar, Y. G. Ma, G. Q. Zhang, and C. L. Zhou, Phys. Rev. C **85**, 024620 (2012).
[34] J. Pu, J. H. Chen, Sanjeev Kumar, Y. G. Ma, C. W. Ma, and G. Q. Zhang, Phys. Rev. C **87**, 047603 (2013).
[35] W. D. Myers and W. J. Swiatecki, Nucl. Phys. A **336**, 267 (1980).
[36] W. D. Myers and K. H. Schmidt, Nucl. Phys. A **410**, 61 (1983).

[37] R. J. Charity, M. A. McMahan, G. J. Wozniak, R. J. McDonald, and L. G. Moretto, Nucl. Phys. A **483**, 371 (1988).
[38] K. Hagel, M. Gonin, R. Wada *et al.*, Phys. Rev. C **50**, 2017 (1994).
[39] W. D. Tian, Y. G. Ma, X. Z. Cai *et al.*, Int. J. Mod. Phys. E **17**, 1705 (2008).
[40] J. Su and F. S. Zhang, Phys. Rev. C **84**, 037601 (2011).
[41] Y. G. Ma, R. Wada, K. Hagel *et al.*, Phys. Rev. C **65**, 051602(R) (2002).
[42] M. Huang, Z. Chen, S. Kowalski, Y. G. Ma *et al.*, Phys. Rev. C **81**, 044620 (2010).
[43] D. Theriault, A. Vallee *et al.*, Phys. Rev. C **71**, 014610 (2005).
[44] M. Mocko, M. B. Tsang, D. Lacroix *et al.*, Phys. Rev. C **78**, 024612 (2008).
[45] M. Mocko, Ph.D. thesis, Michigan State University, 2006.
[46] G. Audi and A. H. Wapstra, Nucl. Phys. A **729**, 337 (2003).
[47] M. Mocko, M. B. Tsang, L. Andronenko *et al.*, Phys. Rev. C **74**, 054612 (2006).
[48] G. A. Souliotis, M. Veselsky, G. Chubarian, L. Trache, A. Keksis, E. Martin, D. V. Shetty, and S. J. Yennello, Phys. Rev. Lett. **91**, 022701 (2003).
[49] C. W. Ma and S. S. Wang, Chin. Phys. C **35**, 1017 (2011).
[50] M. B. Tsang, W. A. Friedman, C. K. Gelbke, W. G. Lynch, G. Verde, and H. S. Xu, Phys. Rev. Lett. **86**, 5023 (2001).
[51] A. S. Botvina, O. V. Lozhkin, and W. Trautmann, Phys. Rev. C **65**, 044610 (2002).
[52] W. D. Tian, Y. G. Ma, X. Z. Cai, D. Q. Fang, W. Guo, W. Q. Shen, K. Wang, H. W. Wang, and M. Veselsky, Phys. Rev. C **76**, 024607 (2007).
[53] M. Veselsky, G. A. Souliotis, and S. J. Yennello, Phys. Rev. C **69**, 031602(R) (2004).
[54] Y. Fu, D. Q. Fang, Y. G. Ma, X. Z. Cai, X. Y. Sun, and W. D. Tian, Nucl. Phys. A **834**, 584c (2010).
[55] G. A. Souliotis, M. Veselsky, D. V. Shetty, and S. J. Yennello, Phys. Lett. B **588**, 35 (2004).
[56] M. Huang, Z. Chen, S. Kowalski *et al.*, Nucl. Phys. A **847**, 233 (2010).
[57] Z. Chen, S. Kowalski, M. Huang, R. Wada *et al.*, Phys. Rev. C **81**, 064613 (2010).
[58] G. A. Souliotis, D. V. Shetty, M. Veselsky, G. Chubarian, L. Trache, A. Keksis, E. Martin, and S. J. Yennello, Phys. Rev. C **68**, 024605 (2003).